INTEGRATED VEHICLE DYNAMICS CONTROL BASED ON CONTROL ALLOCATION WITH SUBSYSTEM COORDINATION

Barys Shyrokau[*1], Danwei Wang[*1] and Markus Lienkamp[*2]
*1 Division of Control and Instrumentation, Nanyang Technological University
50 Nanyang Avenue, S2-B6a-01, Singapore 639798
barys1@e.ntu.edu.sg
*2 TU Muenchen, Lehrstuhl f. Fahrzeugtechnik (FTM)
Boltzmannstr. 15, 85748 Garching, Germany

Abstract

Integrated vehicle dynamics control with the coordination of several vehicle subsystems is considered. The proposed algorithms of subsystem coordination based on restriction weights into the optimal control allocation allow to achieve lower energy consumption without significant impairment of stability of motion and vehicle handling compared with standard control allocation. The proposed control system was investigated using HIL test rig with hardware components of friction brake system and dynamic tire pressure system.

1. INTRODUCTION

Integrated control of multi-actuated vehicle allows to control various operation characteristics such as stability of motion, vehicle handling, energy consumption, ride comfort and others. Due to over-actuated nature, one of the most studied and applied control technique is control allocation [1-3]. Research issues of control allocation cover the following topics as representation of actuator dynamics, approximation of nonlinear allocation, adaptation of control allocation to uncertainties and disturbances and others. In this paper, the emphasis is given to the achievement of several control objectives without complication of cost function.

The aim of this paper is to coordinate/prioritize each vehicle subsystem in accordance with several performance criteria to achieve better vehicle operation characteristics. For this aim, the algorithms based on restriction weights are developed and investigated. The subsystem coordination covers (i) friction brake system, (ii) near-wheel drive electric motors, (iii) wheel steer actuators, (iv) camber angle actuators, (v) dynamic tire pressure system and (vi) actuators generating additional normal forces through external spring, damping and stabilizer forces. The investigated vehicle is a middle-size passenger car with a mass of 1534 kg, weight front/rear distribution 55/45 and tire size 205/60R15.

2. OVERALL CONTROL SYSTEM

The overall structure of control system (Figure 1) consists of a state observer; high-layer control of vehicle dynamics; middle-layer control allocation (CA) and low-layer individual actuator control. Steering angle from driver is the input parameter to the control system. The high layer controller minimizes the deviation between reference and actual vehicle behaviour to guarantee handling and stability of motion. The middle layer allocates control demand between vehicle subsystems. Then the low-layer actuator control guarantees a precise tracking to reference control signals obtained from the middle layer. Moreover, it is used to estimate boundary conditions for control allocation taking into account actuator physical limits and wheel slip control.

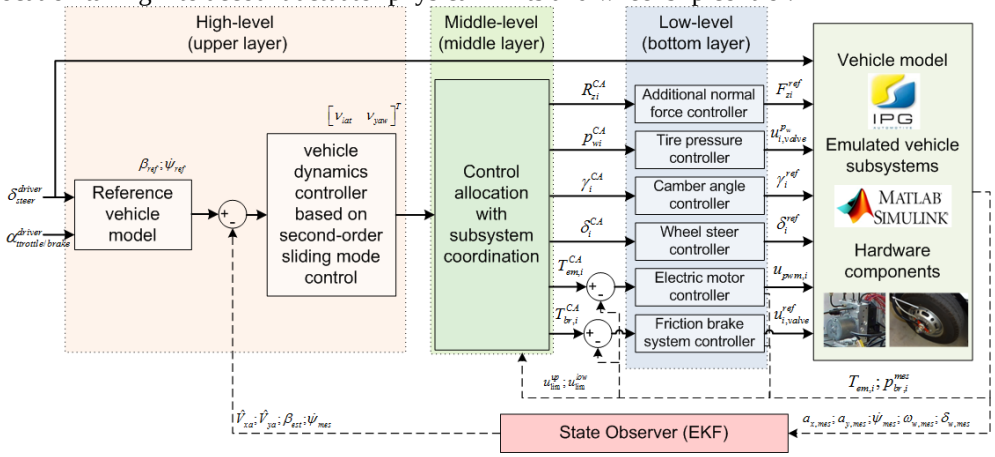

Figure 1 Overall control structure

2.1 High-layer vehicle dynamics controller

The high-layer vehicle dynamics controller consists of two parts: generator of reference signals and vehicle dynamics controller for generation of lateral force and yaw torque demands to minimize a difference between actual and reference vehicle behaviour. The reference signals are reference yaw rate for vehicle handling, and reference sideslip angle, when the vehicle is outside the boundaries of vehicle stability β_{bound} and $\dot{\beta}_{bound}$.

To estimate reference yaw rate, a classical bicycle vehicle model is applied. The reference yaw rate is constrained according to adhesion limits [4]. The controller maintains vehicle stability only during emergency manoeuvres, therefore sideslip angle control should be bounded using phase-plane approach [5]. When sideslip angle is inside the stability boundaries, no action is required. The reference sideslip angle β_{ref} is calculated from estimated β_{est}, boundary β_{bound} and $\dot{\beta}_{bound}$ values as:

$$\beta_{ref} = \begin{cases} \beta_{est} - \beta_{bound}\left(1 - \dfrac{\dot{\beta}_{est}}{\dot{\beta}_{bound}}\right), & \beta_{est} \geq 0 \wedge \dot{\beta}_{est} \geq 0; \qquad \beta_{est} - \beta_{bound}\left(1 + \dfrac{\dot{\beta}_{est}}{\dot{\beta}_{bound}}\right), \quad \beta_{est} \geq 0 \wedge \dot{\beta}_{est} < 0 \\ \beta_{est} + \beta_{bound}\left(1 + \dfrac{\dot{\beta}_{est}}{\dot{\beta}_{bound}}\right), & \beta_{est} < 0 \wedge \dot{\beta}_{est} < 0; \qquad \beta_{est} + \beta_{bound}\left(1 - \dfrac{\dot{\beta}_{est}}{\dot{\beta}_{bound}}\right), \quad \text{otherwise} \end{cases} \tag{1}$$

The control error of sideslip angle e_β and yaw rate $e_{d\psi/dt}$ can be found as:

$$e_\beta = \begin{cases} \left|\beta_{est} - \beta_{ref}\right| \text{sign}\left(\beta_{est}\right), & \beta_{est} > \beta_{ref} \wedge \beta_{ref} > 0 \\ \left|\beta_{est} - \beta_{ref}\right| \text{sign}\left(\beta_{est}\right), & \beta_{est} < \beta_{ref} \wedge \beta_{ref} < 0 \\ 0, \quad \text{otherwise} \end{cases} \qquad e_{\dot{\psi}} = \begin{cases} \dot{\psi}_{ref} - \dot{\psi}_{mes}, & \left|\dot{\psi}_{ref} - \dot{\psi}_{mes}\right| > \Delta_{\dot{\psi}} \\ 0, & \left|\dot{\psi}_{ref} - \dot{\psi}_{mes}\right| < \Delta_{\dot{\psi}} \end{cases} \tag{2}$$

The threshold $\Delta_{\dot{\psi}}$ defines dead zones to eliminate demand generation when control error is insignificant.

The second-order sliding mode control (SOSMC) is selected [6] as the control method to stabilize closed-loop system. Main advantages of SOSMC are chattering reduction and high accuracy under the same robustness in comparison with first-order sliding mode control. The proposed controller is formulated in discrete-time domain, taking into account its subsequent investigation using hardware-in-the-loop (HIL) test rig. To reduce the chattering effect, instead of the application of the sign function in [6], the saturation function is applied.

The generalized lateral force v_{lat} is calculated with sampling time T_s as:

$$v_{lat}\left(k+1\right) = v_{lat}\left(k\right) - K_{sm,\beta} sat\left(f_\beta\right) T_s, \quad \text{sat}\left(f_\beta\right) = \begin{cases} \dfrac{e_\beta\left(k\right) - 0.5 e_{M\beta}\left(k\right)}{\sigma_\beta}, & \left|e_\beta\left(k\right) - 0.5 e_{M\beta}\left(k\right)\right| < \sigma_\beta \\ \text{sgn}\left(e_\beta\left(k\right) - 0.5 e_{M\beta}\left(k\right)\right), & \text{otherwise} \end{cases} \tag{3}$$

The generalized yaw torque v_{yaw} is defined:

$$v_{yaw}\left(k+1\right) = v_{yaw}\left(k\right) - K_{sm,\dot{\psi}}\left(\dot{\psi}\right) sat\left(f_{\dot{\psi}}\right) T_s, \quad \text{sat}\left(f_{\dot{\psi}}\right) = \begin{cases} \dfrac{e_{\dot{\psi}}\left(k\right) - 0.5 e_{M\dot{\psi}}\left(k\right)}{\sigma_{\dot{\psi}}}, & \left|e_{\dot{\psi}}\left(k\right) - 0.5 e_{M\dot{\psi}}\left(k\right)\right| < \sigma_{\dot{\psi}} \\ \text{sgn}\left(e_{\dot{\psi}}\left(k\right) - 0.5 e_{M\dot{\psi}}\left(k\right)\right), & \text{otherwise} \end{cases} \tag{4}$$

Controller gain for generalized yaw torque is proportionally scheduled using values of yaw rate. This procedure reduces the generation of control demand under lower control errors. The controller parameters are related to full vehicle mass m_a and total moment of inertia of vehicle about z-axis I_{zz}. The values of controller gains are obtained from offline-simulation optimization and listed in Table 1.

Table 1 Controller parameters

Sideslip angle control	$K_{sm,\beta} = 10 m_a$; σ_β = 2.5e-2; β_{bound} =3 deg; $\dot{\beta}_{bound}$ = 25 deg/s
Yaw rate control	$K_{sm,\dot{\psi}}\left(\dot{\psi} < 3 \text{ deg/s}\right) = 5 I_{zz}$; $K_{sm,\dot{\psi}}\left(\dot{\psi} > 10 \text{ deg/s}\right) = 25 I_{zz}$; $\sigma_{\dot{\psi}}$ = 5e-2; $\Delta_{\dot{\psi}}$ = 0.25 deg/s

2.2 Middle-layer control allocation

The aim of middle-layer control allocation is a distribution of generalized control demands between vehicle subsystems. The relationship between generalized forces and yaw torque (control demands from high-layer controller) and control input vector (outputs from control allocation) is nonlinear. According to [1, 3] a nonlinear relationship can be linearized about an operating point by first-order Taylor series expansion:

$$v^* = v_d - g\left(\xi, u_{k-1}\right) = \frac{\partial g\left(\xi, u_{k-1}\right)}{\partial u} u_{k-1} \approx B_u\left(\xi, u_{k-1}\right) u_k \tag{5}$$

Tire forces can be separated between forces components related to vehicle motion and subsystem actuation. Neglecting transient processes in actuators and considering their simplified dynamics, the tire force components related to vehicle motion F_{wi}^{sys} and generated by actuators $F_{wi}^{actuators}$ are equal to [7]:

$$\begin{aligned} F_{xwi} &= -\frac{J_{wi}}{r_w}\frac{d\omega_{wi}}{dt} + \frac{1}{r_w}T_{em,i}^{CA} + \frac{1}{r_w}T_{br,i}^{CA} + C_{p_{wx}}p_{wi}^{CA} + C_{Rzx}R_{zi}^{CA} \\ F_{ywi} &= \underbrace{C_{ywi}\left(\tan\frac{V_{yi}}{V_{xi}} - \delta_i^{kinematic}\right)}_{F_{wi}^{sys}} + \underbrace{C_{ywi}\delta_i^{CA} + C_{\gamma i}\gamma_i^{CA} + C_{p_{wy}}p_{wi}^{CA} + C_{Rzy}R_{zi}^{CA}}_{F_{wi}^{actuators}} \end{aligned} \tag{6}$$

The nonlinear component of vehicle motion $g(\xi,u_{k-1})$ can be calculated as:

$$g(\xi,u_{k-1}) = \begin{bmatrix} -m_a V_{xa}\dot{\psi} + \sum_{i=1}^{4} F_{yi}^{sys} \\ a\sum_{i=1}^{2} F_{yi}^{sys} - b\sum_{i=3}^{4} F_{yi}^{sys} + \sum_{i=f,r} t_i \frac{-F_{x,il}^{sys} + F_{x,ir}^{sys}}{2} \end{bmatrix} \tag{7}$$

Since the six vehicle subsystems are considered, and electric motors can develop positive (traction) $T_{em,i}^{CA,pos}$ and negative (brake) $T_{em,i}^{CA,neg}$ torques, the control input vector is given as:

$$u^{CA} = \begin{bmatrix} \delta_i^{CA} & T_{em,i}^{CA,pos} & T_{em,i}^{CA,neg} & T_{br,i}^{CA} & \gamma_i^{CA} & p_{wi}^{CA} & R_{zi}^{CA} \end{bmatrix}^T \tag{8}$$

The control effectiveness matrix B_u is equal to:

$$B_u = \begin{bmatrix} B_\delta & B_{em}^{pos} & B_{em}^{neg} & B_{br} & B_\gamma & B_{p_w} & B_{R_z} \end{bmatrix} \tag{9}$$

The parameters of control effectiveness matrix B_δ for wheel steer actuators δ_i^{CA} can be formulated as:

$$B_\delta = \begin{bmatrix} C_{ywfl}\cos\delta_{fl} & C_{ywfr}\cos\delta_{fr} & C_{ywrl}\cos\delta_{rl} & C_{ywrr}\cos\delta_{rr} \\ C_{ywfl}\chi_{yfl} & C_{ywfr}\chi_{yfr} & C_{ywrl}\chi_{yrl} & C_{ywrr}\chi_{yrr} \end{bmatrix} \tag{10}$$

The kinematic ratios χ_{yi} are:

$$\begin{aligned} \chi_{yfl} &= -0.5t_f\sin\delta_{fl} + a\cos\delta_{fl}; & \chi_{yfr} &= 0.5t_f\sin\delta_{fr} + a\cos\delta_{fr} \\ \chi_{yrl} &= -0.5t_r\sin\delta_{rl} - b\cos\delta_{rl}; & \chi_{yrr} &= 0.5t_r\sin\delta_{rr} - b\cos\delta_{rr} \end{aligned} \tag{11}$$

Control effectiveness matrix B_{br} for friction brake torques $T_{br,i}^{CA}$ can be written using wheel radius r_w:

$$B_{br} = \begin{bmatrix} r_w^{-1}\sin\delta_{fl} & r_w^{-1}\sin\delta_{fr} & r_w^{-1}\sin\delta_{rl} & r_w^{-1}\sin\delta_{rr} \\ r_w^{-1}\chi_{xfl} & r_w^{-1}\chi_{xfr} & r_w^{-1}\chi_{xrl} & r_w^{-1}\chi_{xrr} \end{bmatrix} \tag{12}$$

The kinematic ratios χ_{xi} are:

$$\begin{aligned} \chi_{xfl} &= -0.5t_f\cos\delta_{fl} + a\sin\delta_{fl}; & \chi_{xfr} &= 0.5t_f\cos\delta_{fr} + a\sin\delta_{fr} \\ \chi_{xrl} &= -0.5t_r\cos\delta_{rl} - b\sin\delta_{rl}; & \chi_{xrr} &= 0.5t_r\cos\delta_{rr} - b\sin\delta_{rr} \end{aligned} \tag{13}$$

Control effectiveness matrix B_{pw} for dynamic tire pressures p_{wi}^{CA} is defined as:

$$B_{pw} = \begin{bmatrix} C_{p_{wx}}^{fl}\sin\delta_{fl} + C_{p_{wy}}^{fl}\cos\delta_{fl} & C_{p_{wx}}^{fr}\sin\delta_{fr} + C_{p_{wy}}^{fr}\cos\delta_{fr} & C_{p_{wx}}^{rl}\sin\delta_{rl} + C_{p_{wy}}^{rl}\cos\delta_{rl} & C_{p_{wx}}^{rr}\sin\delta_{rr} + C_{p_{wy}}^{rr}\cos\delta_{rr} \\ C_{p_{wx}}^{fl}\chi_{xfl} + C_{p_{wx}}^{fl}\chi_{yfl} & C_{p_{wx}}^{fr}\chi_{xfr} + C_{p_{wx}}^{fr}\chi_{yfr} & C_{p_{wx}}^{rl}\chi_{xrl} + C_{p_{wx}}^{rl}\chi_{yrl} & C_{p_{wx}}^{rr}\chi_{xrr} + C_{p_{wx}}^{rr}\chi_{yrr} \end{bmatrix} \tag{14}$$

Control effectiveness matrices for electric motors B_{em}^{pos} and B_{em}^{neg} are equal to B_{br}. Control effectiveness matrix B_γ for camber angle actuators γ_i^{CA} is the same as control effectiveness matrix B_δ for wheel steer actuators δ_i^{CA}. Instead of lateral stiffness C_{ywi} the camber stiffness $C_{\gamma i}$ is used. Control effectiveness matrix B_{Rz} for the actuators generating additional normal forces R_{zi}^{CA} is found in the same way as control effectiveness matrix system B_{pw}, when, instead of coefficients C_{pwx} and C_{pwy}, the coefficients C_{Rzwx} and C_{Rzwy} are used.

Tire cornering stiffness C_{ywi}, camber stiffness $C_{\gamma i}$, coefficients C_{pwx} and C_{pwy}, related to changing of longitudinal and lateral force depends on tire pressure, and coefficients C_{Rzwx} and C_{Rzwy}, regarding to longitudinal and lateral force depends on normal forces, are numerically computed as partial derivatives of longitudinal and lateral tire forces from tire model by Taylor series explanation with sampling time of 1ms. The tire model is described by Pacejka tire model including tire inflation/deflation pressures [8].

The control allocation problem is formulated as a minimization of allocation error and control actuations, taking into account actuator constraints [9]:

$$u^{CA} = \arg\min_{u_{\lim}^{low} \le u^{CA} \le u_{\lim}^{up}} \left(\left\| W_\nu (B_u u^{CA} - \nu^*) \right\|_2^2 + \zeta \left\| W_u u^{CA} \right\|_2^2 \right) \tag{15}$$

The parameter ξ defines a significance of minimization of control actuations and equal to 0.1. Matrix W_ν is used to set up a priority among generalized lateral force and yaw torque according to vehicle manoeuvre. A description

of weighting matrix W_u to restrict actuators is described is Section 3. The fixed-point method is selected as optimization solver and it is terminated when the allocation error is lower than predefined tolerance.

Considering only limitation constraints related to longitudinal tire forces for electric motor and frictional brake system since they can generate significantly higher demand compared with dynamic tire pressure system and additional normal force actuators, the limit of longitudinal force F_{xw}^{lim} is calculated from friction circle [4] based on normal and lateral force, and friction coefficient:

$$\begin{aligned} u_{\min}^{tire} &= \begin{bmatrix} 0 & -F_{xw}^{\lim} r_w - T_{br,i} & -F_{xw}^{\lim} r_w \end{bmatrix} \\ u_{\max}^{tire} &= \begin{bmatrix} F_{xw}^{\lim} r_w & 0 & 0 \end{bmatrix} \end{aligned} \tag{16}$$

The actuator position and rates limits are used as optimization constraints to represent static actuator dynamics (Table 2). Since the powertrain architecture has near-wheel motors, the rate limit of torque generated by electric motor is less compared to friction brake system due to low natural frequency of the half-shafts.

Table 2 Position and rate limits of actuators

Subsystem	Position limit	Rate limit
front wheel steer actuators	-30…30 deg	50 deg/sec
rear wheel steer actuators	-15…15 deg	30 deg/sec
camber angle actuators	-10…10 deg	10 deg/sec
electric motor	from torque-speed map	5000 Nm/sec
friction brake system	depends on slip controller	release / build-up 8000 / 12000 Nm/sec
dynamic tire pressure system	1.5 bar	release / build-up 0.6 / 1 bar /sec
additional normal force actuators	1000 N	3000 N/sec

The final constraints for optimization can be written as:

$$u_{\lim}^{low} = \max\left(u_{\min}^{position}, u(T - T_s) - u_{rate} T_s, u_{\min}^{tire}\right) \qquad u_{\lim}^{up} = \min\left(u_{\max}^{position}, u(T - T_s) + u_{rate} T_s, u_{\max}^{tire}\right) \tag{17}$$

2.3 Low-layer actuator control

Low-layer control is used to generate control actuator signals and calculate constraints for middle-layer control allocation. Since the several vehicle subsystems are represented as transfer functions, the reference signals from wheel steer actuators, camber angle actuators and actuators generating additional normal forces are directly assigned to actuator models.

Electric motor controller

The reference signals are e-motor torques obtained from control allocation layer. The detailed description of controller of the electric motor and the position torque limits can be found in [7].

$$u_{pwm,i} = K_p^{em}\left(T_{em,i}^{CA} - T_{em,i}\right) + K_i^{em}\int\left(T_{em,i}^{CA} - T_{em,i}\right)dt \tag{18}$$

Friction brake system controller

The configuration of the brake system incorporates the hydraulic control unit that operates the relay valves. Its control law combines PI gain-scheduling control to demand calculation and rule-based algorithm for demand realization. The brake pressures $p^{mes}{}_{br,i}$ are controlled according to brake torques $T^{CA}{}_{br,i}$ recalculated to reference brake pressures from control allocation layer. The constructive parameters of brakes and the level of wheel slip define the limitation of friction brake torque. Therefore, the position limits for friction brake torque $T_{br,i}^{lim}$ are calculated taking into account the constructive limits $T_i^{constructive}$ and wheel slip. The reactive torque T_{react} is similarly calculated as in [10]:

$$T_{br,i}^{\lim} = \begin{cases} T_i^{constructive}, & s_{wi} < s_w^{threshold} \\ T_{br,i}^{CA} - T_{react}, & s_{wi} > s_w^{threshold} \end{cases} \tag{19}$$

Controller of dynamic tire pressure system

As compared with other actuation systems, the performance of investigated dynamic tire pressure system is slow up to 1 bar/s. The present configuration of the system includes the rule-based controller. The holding time t_{hold} is used to generate step changing of tire pressure, when the error is smaller than 0.5 bar. Valve control signals to the inlet valve $u^{pw}{}_{i,inlet}$ and outlet valve $u^{pw}{}_{i,outlet}$ are defined as:

$$u_{i,inlet}^{pw} = \begin{cases} 1, & \left(p_{w,i}^{ref} - p_{w,i}^{mes} > 0.5\right) \vee \left(p_{w,i}^{ref} - p_{w,i}^{mes} < 0.5 \,\&\, p_{w,i}^{ref} - p_{w,i}^{mes} > 0.1 \,\&\, t_{hold} < 0.02\right) \\ 0, & \left(p_{w,i}^{ref} - p_{w,i}^{mes} < 0.1\right) \vee \left(p_{w,i}^{ref} - p_{w,i}^{mes} < 0.5 \,\&\, p_{w,i}^{ref} - p_{w,i}^{mes} > 0.1 \,\&\, t_{hold} > 0.02\right) \end{cases}$$
$$u_{i,outlet}^{pw} = \begin{cases} 1, & \left(p_{w,i}^{ref} - p_{w,i}^{mes} > -0.5\right) \vee \left(p_{w,i}^{ref} - p_{w,i}^{mes} < -0.5 \,\&\, p_{w,i}^{ref} - p_{w,i}^{mes} > -0.1 \,\&\, t_{hold} < 0.02\right) \\ 0, & \left(p_{w,i}^{ref} - p_{w,i}^{mes} < -0.1\right) \vee \left(p_{w,i}^{ref} - p_{w,i}^{mes} < -0.5 \,\&\, p_{w,i}^{ref} - p_{w,i}^{mes} > -0.1 \,\&\, t_{hold} > 0.02\right) \end{cases} \quad (20)$$

3. SUBSYSTEM COORDINATION

3.1 Concept of vehicle subsystem prioritization

The multi-actuator configuration allows to use various subsystems to generate control demand for the compensation of control errors. Several authors noted [2,5], the combination of various vehicle subsystems helps to achieve better operation characteristics in the comparison with stand-alone operation.

The research idea of this paper is to coordinate / prioritize each vehicle subsystem, when control demand is developed, in accordance with some performance criteria, which is related to vehicle operation characteristics. On the left-hand graph of Figure 2 illustrative example of the demand distribution is shown, when all vehicle subsystems have the same priority. As a result, the ratios between demands v_1, v_2 and v_3 are constant. The right-hand graph of Figure 2 demonstrates a situation when priority of each subsystem changes according to the performance criterion. In this case, the ratios between demands v_1, v_2 and v_3 are different. Their values depend on which subsystem has higher priority for the current range of performance criterion. For explanation, three subsystems are considered, which form a certain control demand like generalized yaw torque. If the performance criterion, for example, control error of yaw rate, is small, the control demand will be mainly generated only by steering and drive system. It allows to reduce the usage of the friction brake system to decrease non-recuperative energy losses. When the level of control error is increased, the participation of the friction brake system rises, because steering and drive subsystems cannot develop control demand precisely due to the position and rate limits.

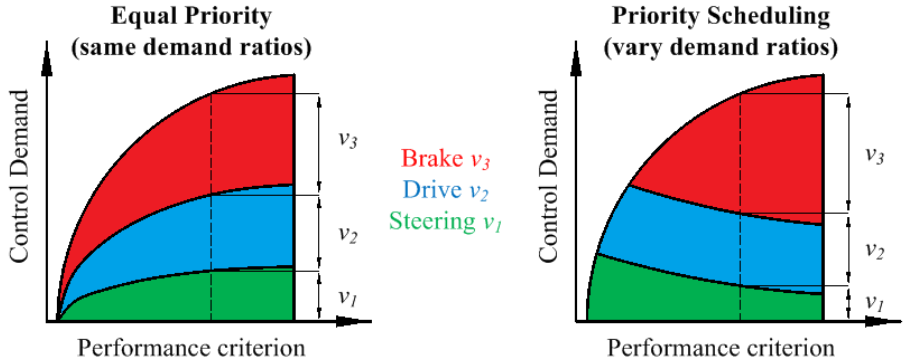

Figure 2 Illustrative example of actuator coordination/prioritization

3.2 Proposed algorithms of subsystem coordination

The aim of proposed algorithms is to define restriction weights w_{ui} into the matrix W_u (15) for subsystem prioritization. The restriction weights should be changed according to performance criteria, which can characterize energy consumption and energy losses. The advantage of this approach is the solution of multi-objective problem without the supplying of auxiliary cost terms into the cost function. Thereby, the computational budget does not increase; however, the drawback relates to pre-designed definition of restriction weights and their influence on performance criteria based on offline-simulations.

Performance criteria and manoeuvre for weight definition

The criteria allowing real-time assessment of energy consumption and energy losses should be primarily formulated. To evaluate tire energy dissipation from longitudinal forces, the dimensionless criterion η_{lon}, called longitudinal efficiency, is introduced. It demonstrates the net longitudinal power, which can be potentially realized into tire-road contact without longitudinal slip losses:

$$\eta_{lon} = 1 - \frac{\sum_{i=1}^{4} \left| \hat{F}_{xwi} \hat{V}_{swi} \right|}{\sum_{i=1}^{4} \left| \hat{F}_{xwi} \hat{V}_{xwi} \right|} \quad (21)$$

To evaluate tire energy dissipation from lateral forces, the dimensionless criterion η_{lat}, called lateral efficiency, is used. It represents the net lateral power, which is limited by maximal lateral forces of linear vehicle model. The lateral slip angle α_w^{net},, corresponding to maximum pure cornering force of linear vehicle mode, is pre-defined and equal to 8^0 in accordance with analysis of reference data [4]:

$$\eta_{lat} = 1 - \frac{\sum_{i=1}^{4} \left| \hat{F}_{ywi} \hat{V}_{ywi} \right|}{0.5 \left(C_f \sum_{i=1}^{2} \left| \hat{V}_{xwi} \right| + C_r \sum_{i=3}^{4} \left| \hat{V}_{xwi} \right| \right) \alpha_w^{net} \tan \alpha_w^{net}} \tag{22}$$

Energy consumed by electric motor is much higher as total energy demand of actuators of the remaining subsystems. Since the manoeuvres of short duration are further considered, energy consumption of other actuators is neglected. The criterion η_{con} related to power consumption and criterion η_{rec} related to potential power recuperation of electric motor are introduced:

$$\eta_{con} = 1 - \frac{\sum_{i=1}^{4} \max\left(0, P_{em,i}\right)}{4 P_{e\max}} \qquad \eta_{rec} = 1 - \frac{\sum_{i=1}^{4} \left| \min\left(0, P_{em,i}\right) \right|}{4 P_{e\max}} \tag{23}$$

To analyze how selected criteria depend on restriction weight and to develop algorithms of the subsystem coordination, the modified ‘Step Steer’ manoeuvre with initial velocity of 100 km/h and steer amplitude of 70 deg is used. The modified open-loop manoeuvre is implemented without the control of vehicle velocity in comparison with standard one. Simulation procedures are sequentially carried out for several vehicle configurations. Each vehicle configuration has only one specified vehicle subsystem activated during the manoeuvre. The control of other available subsystems is disabled. The upper part of Figure 3 shows corresponding results of stand-alone operation of vehicle subsystems with the restriction weights w_{ui} equal to one. The bottom part of Figure 3 represents relationships between mean values of performance criteria and restriction weight for each subsystem.

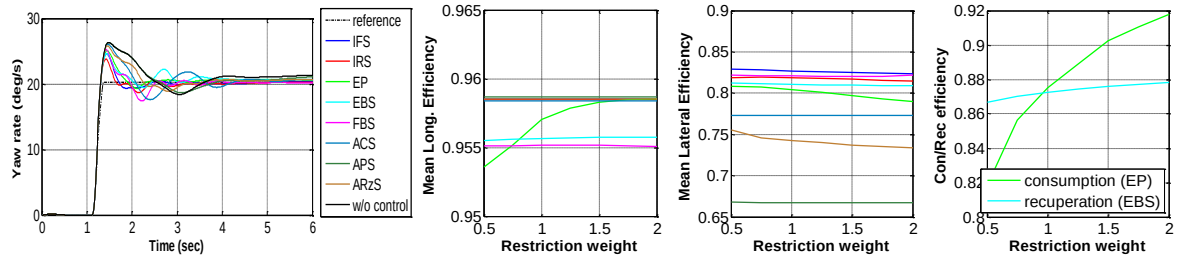

Figure 3 Longitudinal and lateral efficiency, consumption and recuperation efficiency versus restriction weight IFS – individual front wheel steering; IRS – individual rear wheel steering; EP – traction torques generated by electric motors; EBS – brake torques generated by electric motors; FBS – friction brake system; ACS – active camber system; APS – dynamic tire pressure system; ARzS – additional normal forces generated by external spring, damping and stabilizer forces.

Using the relationships between mean values of performance criteria and restriction weight from simulation results of the series of modified ‘Step Steer’ manoeuvres, the algorithms of dynamic change of restriction weights can be proposed.

Approach 1: Fuzzy-based subsystem coordination, called ‘fuzzy’

The first approach is based on soft-computing technique, which allows to define control laws without exact mathematical formulation. The membership functions for input parameters – longitudinal and lateral efficiency, consumption and recuperation efficiency – are formulated (Figure 4, a-d). The membership functions of restriction weight for each vehicle subsystem are the identical and shown in Figure 4e. The fuzzy rules from Table 3 cover the most significant relationships between input and output parameters. They are defined using heuristic analysis of performance criteria behaviour under different restriction weights. Criteria η_{con} and η_{rec} and corresponding fuzzy rules are relevant only to the electric motor.

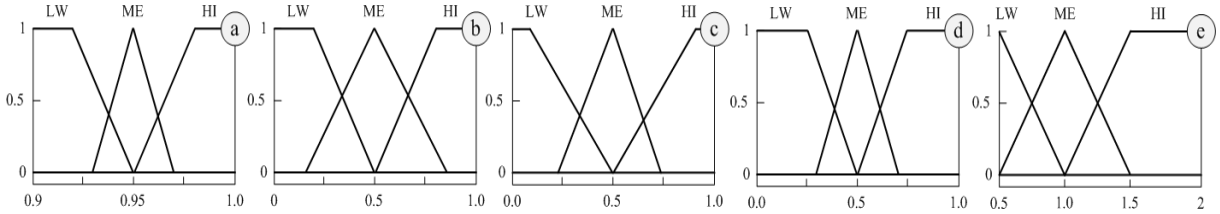

Figure 4 Membership functions for: a) longitudinal efficiency, b) lateral efficiency, c) consumption efficiency, d) recuperation efficiency, e) restriction weight

Table 3 Fuzzy rules

η_{lon}	η_{lat}	η_{con}	η_{rec}	w_{ifs}	w_{irs}	w_{ep}	w_{ebs}	w_{fbs}	w_{acs}	w_{aps}	w_{aRzs}
LW	LW			HI	HI	HI	LW	LW	HI	LW	LW
	ME			ME	ME	HI	LW	LW	ME	ME	ME
	HI			LW	LW	HI	LW	LW	LW	HI	HI
ME	LW			HI	HI	ME	ME	ME	HI	LW	LW
	ME	-	-	ME	ME	ME	ME	ME	ME	ME	ME
	HI			LW	LW	ME	ME	ME	LW	HI	HI
HI	LW			HI	HI	LW	HI	HI	HI	LW	LW
	ME			ME	ME	LW	HI	HI	ME	ME	ME
	HI			LW	LW	LW	HI	HI	LW	HI	HI
-	-	LW	-	-	-	HI	-	-	-	-	-
		ME				ME					
		HI				LW					
		-	LW			-	LW				
			ME				ME				
			HI				HI				

Approach 2: Single iteration subsystem coordination, called 'iterative'

The second approach is based on an iterative procedure of subsystem coordination. The number of considered vehicle subsystems is higher than the number of performance criteria, therefore, the system is underdetermined. Moreover, an exact formulation of the relationships between performance criteria and restriction weights during vehicle motion is the complex task to be mathematically described. Therefore, mean values of performance criteria can be used as qualitative indicators of these relationships. It has been proved with simulation results of modified 'Step Steer' manoeuvre (Figure 3). Next paragraphs introduce how to detect links between performance criteria and restriction weights by the example of lateral efficiency. It is further assumed that: (i) current value of performance criterion is linked to mean value and restriction weight; (ii) current value of performance criterion can be represented as a linear product between ratio $\chi(\bar{\eta}_i)$ and restriction weight w_i.

As an example, the relationship between lateral efficiency and restriction weight is:

$$\eta_{lat} = f(\bar{\eta}_{lat}, w_i) = \chi(\bar{\eta}_{lat}) w_i = B_{wui} w_i \tag{24}$$

The control effectiveness matrix B_{wui} combining the ratios $\chi(\bar{\eta}_{lon})$, $\chi(\bar{\eta}_{lat})$, $\chi(\bar{\eta}_{con})$ and $\chi(\bar{\eta}_{rec})$ is represented as rescaled polynomials obtained from Figure 5. The shift of each characteristic depends on current value of performance criteria. The variation of longitudinal efficiency ratio $\chi(\bar{\eta}_{lon})$ is scaled taking into account the range of criterion changing from 0.9 to 1 for the manoeuvre like 'Step Steer'.

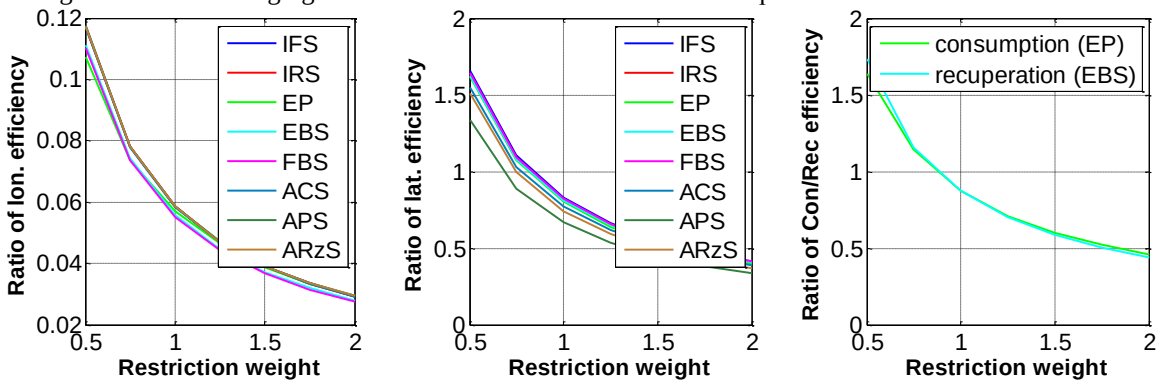

Figure 5 Ratio χ_i versus restriction weight for each vehicle subsystem

To find restriction weight for each actuator, the similar approach as control allocation problem (Eq. 15) is used. Only allocation error between current performance criteria and restriction weights should be minimized. The input vector v_w includes performance criteria taking into account a number of vehicle subsystems N_{subs}:

$$v_w = \begin{bmatrix} N_{subs}\eta_{lon} & N_{subs}\eta_{lat} & \eta_{con} & \eta_{rec} \end{bmatrix}^T \tag{25}$$

Then the vector w_u representing subsystems' restriction weights can be calculated as:

$$w_{u,i+1} = \underset{0.5 \le w_{u,i+1} \le 2}{sat} \left(\frac{B_{wui}^T W_v^w v_w}{\left\| B_{wui}^T W_v^w B_{wui} \right\|_2} - \left(\frac{B_{wui}^T W_v^w B_{wui}}{\left\| B_{wui}^T W_v^w B_{wui} \right\|_2} - I_{4x4} \right) w_{u,i} \right) \tag{26}$$

The range of weight variation is saturated in the interval from 0.5 to 2. To eliminate an effect of noisy behaviour or sharp change of the subsystem priority, the rate of weight changing is added into the algorithm. The matrix W_v^w can be used to define a priority of each performance criterion.

4. HARDWARE-IN-THE-LOOP (HIL) TESTING

4.1 Hardware components of the test rig

Friction brake system of the HIL test rig is conventional brake system, which consists of the master cylinder, four brake assemblies and hydraulic control unit and pressure sensors, which allow measurement of brake pressure in each circuit as well as in each brake caliper. Dynamic tire pressure system allows to control each individual tire pressure, taking into account static load on each wheel and constructive features of the system like pneumatic line lengths [11].

Figure 6 Hardware components of the test rig [11]

4.2 Computational models of vehicle subsystems

The vehicle subsystems and components like electric powertrain, wheel steer actuators, camber angle actuators and actuators generating additional normal forces have software realization in MATLAB/Simulink and can interface with the described hardware subsystems. The HIL test rig has the interface with the IPG CarMaker software environment allowing the embedding of a full vehicle and subsystem simulators.

The model of an electric motor includes steady-state behaviour by a look-up table of motor characteristics and transient behaviour. The transient behaviour of the electric motor is represented by the first-order transfer function with time delay as [12]:

$$T_{em,i} = \frac{T_{em,i}^{ss}}{0.0022s+1} e^{-0.002s} \tag{27}$$

The driveline layout consists of near-wheel electric motors with single-stage transmission and half-shafts to transmit output torque from electric motor to the wheel. The transmission dynamics can be described as [12]:

$$\left(J_{em} + J_{tr1} + \frac{u_{tr}^2}{\eta_{tr}} \left(J_{tr2} + \frac{0.5 J_{hs}}{\eta_{joint}^{inner}} \right) \right) \ddot{\theta}_{em,i} = T_{em,i} - \frac{u_{tr}}{\eta_{tr}} T_{hs,i} \tag{28}$$

The half-shaft torques $T_{hs,i}$ and transmitted torque T_{wi} to the wheel by the half-shaft are calculated as [12]:

$$T_{hs,i} = K_{hs}\left(u_{tr}\omega_{em,i} - \omega_{wi}\right) + C_{hs}\left(u_{tr}\theta_{em,i} - \theta_{wi}\right) \qquad 0.5 J_{hs}\ddot{\theta}_{w,i} = T_{hs,i} - \frac{T_{wi}}{\eta_{joint}^{outer}} \tag{29}$$

The external front and rear angles generated by wheel steer actuators are recalculated in accordance with [13]:

$$\frac{\delta_{f,i}^{ext}}{\delta_{f,i}^{ref}} = \frac{1}{0.01s+1} e^{-0.002s}, i = 1,2; \qquad \frac{\delta_{r,i}^{ext}}{\delta_{r,i}^{ref}} = \frac{1}{2.53\cdot 10^{-4} s^2 + 0.011s + 1} e^{-0.003s}, i = 3,4 \tag{30}$$

Since only the prototypes of camber angle actuators are known, the information regarding actuation frequency and delays is varied in the wide range. The prototype of active camber system [14] allows to realize a camber actuation time of 0.3 s. The transfer function of camber angle actuator is selected as:

$$\frac{\gamma_i^{ext}}{\gamma_i^{ref}} = \frac{1}{0.15s+1} e^{-0.020s} \tag{31}$$

To change distribution of normal forces, the variable stiffness suspension, electrorheological dampers and electromechanical anti-roll bars can be applied. The dynamics of variable stiffness suspension is described as [15]:

$$\frac{F_{spring,i}^{ext}}{F_{spring,i}^{ref}} = \frac{1}{0.03s+1} e^{-0.008s} \tag{32}$$

Since electrorheological dampers are considered instead of semi-active hydraulic dampers, the dynamics of active damping system will be faster [16]:

$$\frac{F_{damp,i}^{ext}}{F_{damp,i}^{ref}} = \frac{1}{0.005s+1} e^{-0.005s} \tag{33}$$

The dynamics of active anti-roll bar depends on type of actuator. For electromechanical actuator of active anti-roll bar time constant is experimentally around 50 ms [17]. The several publications propose to use time constant from 20-60 ms [13]. The system dynamics is represented by:

$$\frac{F_{arb,i}^{ext}}{F_{arb,i}^{ref}} = \frac{1}{0.05s+1} e^{-0.010s} \tag{34}$$

5. HIL TEST RIG EXPERIMENTAL RESULTS

The manoeuvre is 'Sine with Dwell' at initial velocity of 80 km/h and steering amplitude of 120 deg on dry asphalt. The motion characteristics are shown in Figure 7 and subsystem actuations for 'iterative' algorithm are in Figure 8.

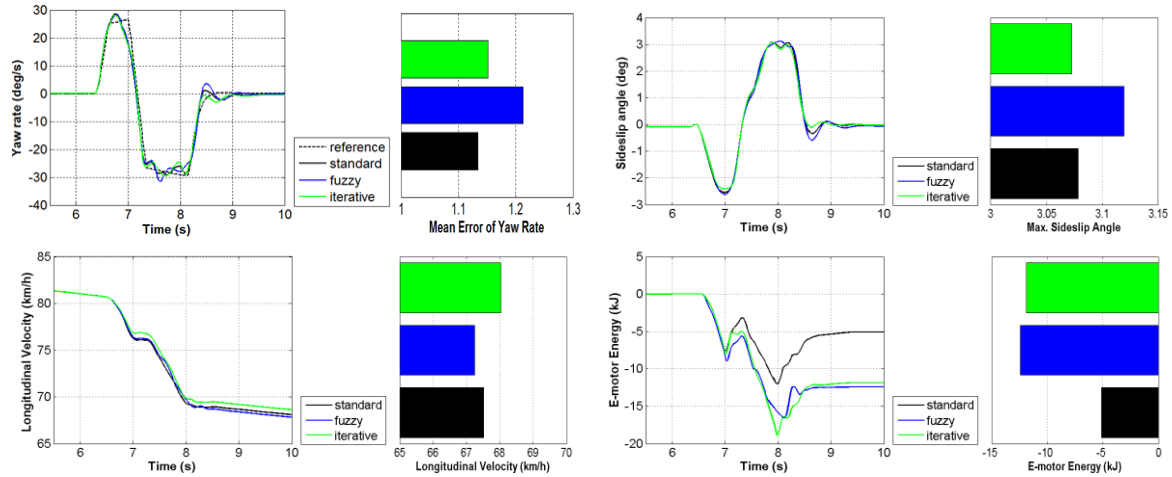

Figure 7 HIL test rig results during 'Sine with Dwell' manoeuvre

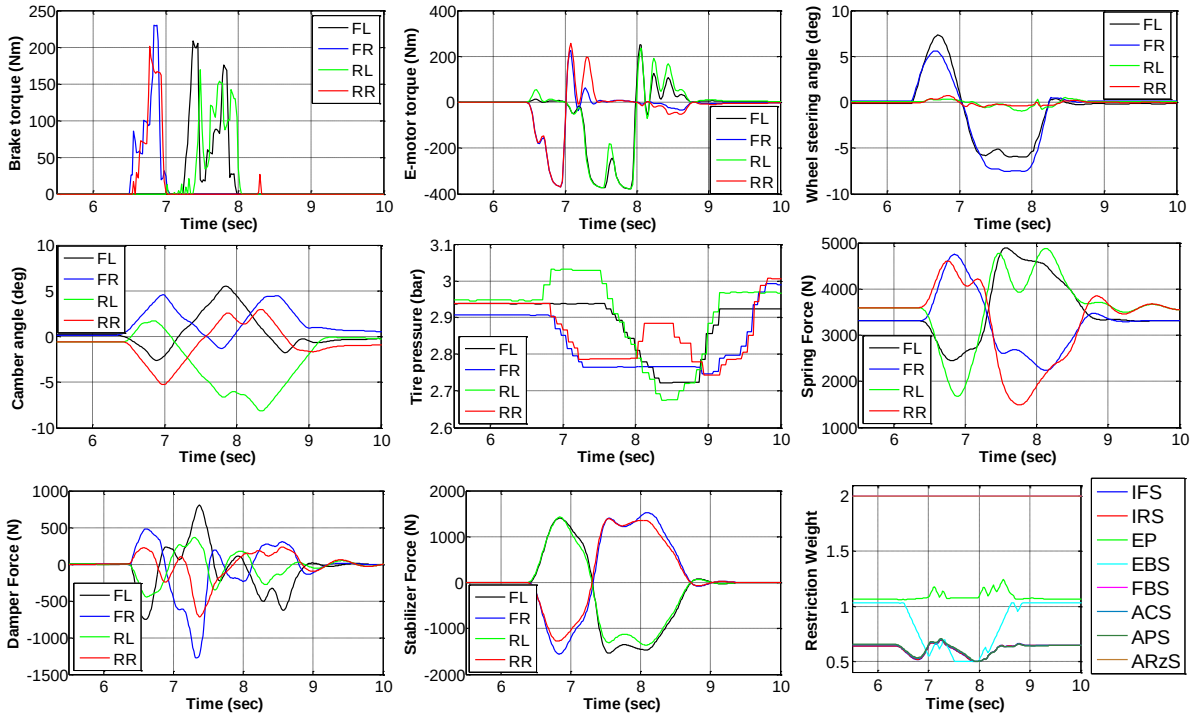

Figure 8 Subsystem actuations during 'Sine with Dwell' manoeuvre for 'iterative' algorithm

The experimental results of yaw rate and sideslip angle demonstrate that all variants guarantee stability of vehicle motion. Comparing to the motion without subsystem coordination, the mean error of yaw rate is 6.5% higher for 'fuzzy' variant and 1.2% higher for 'iterative'. The maximum of sideslip angle is 1.3% higher for 'fuzzy', and 0.9% lower for 'iterative' compared with 'standard' without the changing of restriction weights. The longitudinal velocity at the end of manoeuvre for all considered variants is relative same. The maximal

longitudinal velocity of 68.3 km/h is reached for ‘iterative’, which is 1.1% higher than ‘standard’. However, for all variants with subsystem coordination the value of potential recuperated energy is roughly 2.5 times higher, compared to ‘standard’. Negative value means potential energy, which can be potentially recuperated. The growth of the value of potential recuperated energy is caused by the redistribution effect: participation of electric motors and wheel steer actuators is increased at the sacrifice of friction brake application.

6. CONCLUSIONS

The paper describes the development and evaluation of a control system with subsystem coordination for a multi-actuated vehicle. The algorithms of subsystem coordination based on restriction weights into the control allocation are proposed. The restriction weights are changed according to performance criteria characterizing energy consumption and energy losses. For ‘Sine with Dwell’ manoeuvre, the investigations of proposed algorithms were carried out by means of hardware-in-the-loop test rig with hardware components of conventional brake system and dynamic tire pressure system in real-time domain. Both algorithms demonstrate a relative rise in potential recuperated energy while keeping other vehicle operation characteristics close to ordinary control allocation, when subsystem coordination is missing.

7. ACKNOWLEDGMENT

This publication is made possible by the Singapore National Research Foundation under its Campus for Research Excellence And Technological Enterprise (CREATE) programme. The views expressed herein are solely the responsibility of the authors and do not necessarily represent the official views of the Foundation. This work is also supported in part by National Natural Science Foundation of China (91120308). The authors also would like to thank the Department of Automotive Engineering at Ilmenau University of Technology for experimental facilities and, especially, Dipl.-Ing. Dzmitry Savitski for his help with experimental investigations.

References

[1] J. Wang and R. G. Longoria, "Coordinated and Reconfigurable Vehicle Dynamics Control," IEEE Transactions on Control Systems Technology, vol. 17, pp. 723-732, 2009.
[2] S. Yim, J. Choi and K. Yi, "Coordinated Control of Hybrid 4WD Vehicles for Enhanced Maneuverability and Lateral Stability," IEEE Transactions on Vehicular Technology, vol. 61, pp. 1946-1950, 2012.
[3] A. Hac, D. Doman and M. Oppenheimer, "Unified Control of Brake- and Steer-by-Wire Systems Using Optimal Control Allocation Methods," SAE Technical Paper, 2006-01-0924.
[4] R. Rajamani, Vehicle dynamics and control: Springer, 2011.
[5] J. He, D. A. Crolla, M. C. Levesley and W. J. Manning, "Coordination of active steering, driveline, and braking for integrated vehicle dynamics control," Proc IMechE Part D: J Auto. Eng., vol. 220, pp. 1401-1421, 2006.
[6] G. Bartolini, A. Pisano and E. Usai, "Digital second order sliding mode control of SISO uncertain nonlinear systems," American Control Conference, 1998, pp. 119-124.
[7] B. Shyrokau and D. Wang, "Coordination of Steer Angles, Tyre Inflation Pressure, Brake and Drive Torques for Vehicle Dynamics Control," SAE Int. J. Passeng. Cars - Mech. Syst., vol. 6, pp. 241-251, 2013.
[8] I. Besselink, A. Schmeitz, and H. Pacejka, "An improved Magic Formula/Swift tyre model that can handle inflation pressure changes," Vehicle System Dynamics, vol. 48, pp. 337-352, 2010.
[9] O. Härkegård, "Backstepping and control allocation with applications to flight control," PhD thesis, Linköpings universitet, 2003.
[10] V. Ivanov, B. Shyrokau, K. Augsburg and S. Gramstat, "Advancement of vehicle dynamics control with monitoring the tire rolling environment," SAE Int. J. Passeng. Cars - Mech. Syst., vol. 3, pp. 199-216, 2010.
[11] L. Heidrich, B. Shyrokau, D. Wang, D. Savitski and V. Ivanov, "Hardware-in-the-loop test rig for integrated vehicle control systems," 7th IFAC Symposium on Advances in Automotive Control, Tokyo, Japan, 2013
[12] F. Bottiglione, A. Sorniotti and L. Shead, "The effect of half-shaft torsion dynamics on the performance of a traction control system for electric vehicles," Proc IMechE Part D: J Auto. Eng., vol. 226, no.9, pp. 1145-1159, 2012.
[13] A. Lee, "Coordinated control of steering and anti-roll bars to alter vehicle rollover tendencies," Journal of Dynamic Systems, Measurement, and Control, vol. 124, pp. 127-132, 2002.
[14] M. Horiguchi, A. Mizuno, M. Jones and K. Futamura, "Active Camber Control," FISITA 2012 World Automotive Congress, 2013, pp. 247-256.
[15] A. Alleyne, "Improved vehicle performance using combined suspension and braking forces," Vehicle System Dynamics, vol. 27, pp. 235-265, 1997.
[16] J. Dixon, The shock absorber handbook: Wiley, 2007.
[17] Sorniotti, A., "Electro-Mechanical Active Roll Control: A New Solution for Active Suspensions," SAE Technical Paper 2006-01-1966, 2006.